Biophysical Journal

Volume 101
Number 6

September 21, 2011

www.biophysj.org

Biophysical Society

Published by Cell Press
for the Biophysical Society

In Vivo Measurement of Age-Related Stiffening in the Crystalline Lens by Brillouin Optical Microscopy

Giuliano Scarcelli,[†‡] Pilhan Kim,[†‡] and Seok Hyun Yun[†‡§*]

[†]Wellman Center for Photomedicine, Massachusetts General Hospital, Boston, Massachusetts; [‡]Department of Dermatology, Harvard Medical School, Boston, Massachusetts; and [§]Division of Health Sciences and Technology, Harvard-Massachusetts Institute of Technology, Cambridge, Massachusetts

ABTRACT The biophysical and biomechanical properties of the crystalline lens (e.g., viscoelasticity) have long been implicated in accommodation and vision problems, such as presbyopia and cataracts. However, it has been difficult to measure such parameters noninvasively. Here, we used in vivo Brillouin optical microscopy to characterize material acoustic properties at GHz frequency and measure the longitudinal elastic moduli of lenses. We obtained three-dimensional elasticity maps of the lenses in live mice, which showed biomechanical heterogeneity in the cortex and nucleus of the lens with high spatial resolution. An in vivo longitudinal study of mice over a period of 2 months revealed a marked age-related stiffening of the lens nucleus. We found remarkably good correlation (log-log linear) between the Brillouin elastic modulus and the Young's modulus measured by conventional mechanical techniques at low frequencies (~1 Hz). Our results suggest that Brillouin microscopy is potentially useful for basic and animal research and clinical ophthalmology.

INTRODUCTION

The crystalline lens in the eye plays a central role in vision. Together with the cornea, the lens is responsible for transmitting and focusing incoming light onto the retina (1). The lens is made up of elongated fiber cells with no nuclei and no mitotic activity (2), and continues to grow throughout life without discarding or replacing old cells (3). When new cells are formed in the epithelium and differentiate into fiber cells into the cortex, old cells are packed toward the nucleus with tighter spacing as age advances. This results in a shell structure of fiber layers packed with increasing density toward the nucleus, giving rise to the remarkable optical properties, such as transparency and a radial gradient of refractive index, that are necessary for normal vision (4–6). The microstructure is also closely related to the biomechanical properties of the lens, which play an important role in biotransport as well as visual accommodation (7).

The specific biomechanical properties of the lens and their alterations by aging have been linked to some important ocular problems, such as presbyopia and cataracts (8,9). Presbyopia, the loss of accommodation power, affects most of the population above 40–50 years of age. Age-related increases in the stiffness of the lens are thought to be the primary cause of presbyopia (8,10–12), because stiffer lenses are more resistant to the compression and tension given by the ciliary muscle (13). Age-related nuclear cataracts, characterized by abnormal protein oxidation, cross-linking, and coloration in the nucleus, are the leading cause of blindness worldwide. The pathogenesis of this disorder is not fully understood, but it has been linked to the reduced transport of small molecules, such as antioxidants, in the lens due to an increased viscoelastic modulus and tight packing of lens fibers (9,14).

Investigators have shown considerable interest in measuring the mechanical properties of the crystalline lens for basic research and early diagnosis, and potentially for surgical intervention and therapy for presbyopia (12,15,16). Several studies have demonstrated age-related stiffening of excised human and animal lenses by using various testing tools, such as a spinning cup (17), mechanical stretchers (18), stress-strain equipment (19,20), and bubble-based acoustic radiation force (21). Ultrasound has also been used to measure the spatial variation of packing density inside the lens ex vivo (22).

Here we report for the first time, to our knowledge, the in vivo measurement of the mechanical properties of a crystalline lens. For this study, we optimized a Brillouin optical microscope that was recently developed in our laboratory (23) for the characterization of animal lenses. This noncontact optical method allowed us to obtain a high-resolution, three-dimensional (3D) map of the elastic modulus of the lens in live mice. From a longitudinal study, we obtained the first in vivo direct evidence regarding age-related stiffening of murine lenses. Furthermore, we performed a validation study in which we compared the Brillouin measurements with respect to standard mechanical tests, and the results provided novel insights into the relationship between the hypersonic acoustic properties and conventional rheological moduli measured at much lower frequencies.

Spontaneous Brillouin light scattering arises from the interaction between photons and acoustic phonons (i.e., propagation of thermodynamic fluctuations). A small sample volume (10 pL to 100 nL) can be probed optically in the back-scattering configuration (Fig. 1 *a*). The excitation and relaxation of acoustic phonons induce a positive and negative frequency

Submitted March 14, 2011, and accepted for publication August 3, 2011.

*Correspondence: syun@hms.harvard.edu

Editor: David E. Wolf.

0006-3495/11/09/1539/7 $2.00

doi: 10.1016/j.bpj.2011.08.008

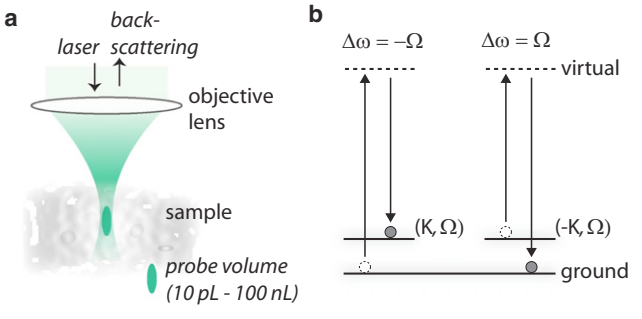

FIGURE 1 Brillouin light scattering microscopy: principle, setup, and characterization. (*a*) Probing volume. (*b*) Conceptual energy diagram of photon-phonon interaction in spontaneous Brillouin scattering. (*c*) Schematic of the confocal microscope setup.

shift by $\Omega = V/\Lambda$ (Fig. 1 *b*), where V is the propagation speed of acoustic phonon and Λ is the phonon wavelength that satisfies the phase matching condition: $\Lambda=\lambda/2n$, where λ is the optical wavelength in air and n is the refractive index. For visible light, Λ is 100–250 nm and Ω is on the order of 10 GHz. The elastic modulus, M', is expressed as $M'=\rho\lambda^2\Omega^2/(4n^2)$, where ρ is the mass density. Therefore, with the known (or estimated) local value of ρ/n^2 of a sample, the longitudinal modulus can be computed from the Brillouin frequency shift that is measured directly by optical spectroscopy. In combination with a confocal setup, this technique allows for biomechanical imaging (23). Brillouin spectroscopy has been applied to the characterization of biological samples, including ocular tissues ex vivo and polymeric specimens in vitro (24,25). To our knowledge, however, in vivo Brillouin measurement has not heretofore been demonstrated.

MATERIALS AND METHODS

Brillouin confocal microscope

Fig. 1 *c* shows a schematic of the Brillouin microscope. The light source is a frequency-doubled Nd-YAG laser (Torus; Laser Quantum. Stockport, UK) emitting a single frequency mode at 532 nm. The laser beam was expanded to 7.5 mm diameter ($1/e^2$) and then focused to the sample by an aspheric lens with a long focal length (f = 35 mm; Edmund Optics, Barrington, NJ). The resulting confocal resolution was ~$4(x) \times 4(y) \times 100(z)$ μm^3. For 3D imaging, the sample was translated stepwise using three-axis motorized stages (Zaber Technologies, Vancouver, British Columbia, Canada, and NewFocus, Irvine, CA). Scattered light from the samples was collected by a single-mode optical fiber (Thorlabs, Newton, NJ) serving as a confocal pinhole, and delivered to a VIPA spectrometer.

VIPA spectrometer

The spectrometer consists of two cascaded VIPA stages (see Supporting Material) with a relay telescope and square-aperture spatial filter in between (26,27). The two VIPA etalons have identical specifications (R1 = 99.9%, R2 = 95%, 1.6° tilt; LightMachinery, Nepean, Ontario Canada). The diffraction pattern after the final VIPA stage was detected with the use of an EM-CCD camera (Ixon Du197; Andor, Belfast, Northern Ireland) with a dispersion slope of 0.5 GHz/pixel.

Data acquisition and analysis

We used LABVIEW for instrument automation (e.g., controlling translational stages, camera, and shutters) and MATLAB (The MathWorks, Natick, MA) for spectral analysis. Our algorithm determines the spectral dispersion axis, extracts the optical spectrum, and measures the Brillouin shift and magnitude by curve-fitting with Lorentzian profiles. We produced Brillouin images in MATLAB using the hot color map. For the conversion from Brillouin frequency shift to the Brillouin longitudinal modulus, we used ρ = 1.13g/cm^3 and n = 1.4 for porcine lenses in the analysis shown in Fig. 6 (22,28), and ρ = 1.18g/cm^3 and n = 1.43 for bovine lenses used in Figs. 5 and 6 (29,30). We estimate that the conversion error due to sample-to-sample variations in ρ/n^2 is relatively small and does not affect the correlation between the Brillouin modulus and Young's modulus (see Supporting Material).

In vivo measurement of the eye

Mice (C57BL/6 strain, 2 weeks to 18 months old) were anesthetized by an intravenous injection of pentobarbital. Tropicamide 1% was administered to dilate the pupil. A piece of coverslip was attached to the cornea with Methocel to prevent drying and minimize optical refraction at the corneal surface. The mouse was placed in a heated tube during the Brillouin measurement. All animal experiments were performed in compliance with institutional guidelines and approved by the subcommittee on research animal care at Massachusetts General Hospital.

Sample preparations for mechanical measurements

We surgically extracted lenses from fresh porcine and bovine eyeballs (Research 87) and carefully removed the lens capsules. To measure the bovine lens nucleus (see Fig. 5, *b* and *c*), we first used a biopsy punch to extract tissue columns (6 mm diameter, 7–10 mm long) and then used razor blades to extract central pieces of 3 mm in each side. To measure the swine lenses (see Fig. 6 *a*), we obtained small pieces of swine lenses of various ages in cube shapes (~5×5×3 mm^3) from various regions of the lens, including the cortex and nucleus, using razor blades. The measurement data shown in Fig. 6 *b* were obtained with the central cylindrical columns extracted by using the biopsy punch from bovine lenses.

Mechanical measurements of lenses ex vivo

On each batch of samples, we performed Brillouin, stress-strain, and shear tests, all within 12 h postmortem. For Brillouin tests, we measured nine depth profiles (spaced 50 μm in the x-y directions) around the center of the lens. We then averaged the peak frequency shift from each depth profile, from which the representative Brillouin nuclear modulus was computed. We performed the stress-strain tests at constant strain rates (1–5% strain per minute) by using a standard instrument (Instron 5542) with compressive plates of 50 mm diameter. We calculated the Young's modulus by linear fitting of the stress-strain curves up to 5% strain. For shear rheometry, we used a standard stress-controlled rheometer (AR-G2; TA Instruments)

with 20-mm-diameter parallel plate geometry. At 200 μm precompression, we performed frequency sweeps from 0.1 to 50 Hz with 0.1% strain amplitude at 23°C.

RESULTS

In vivo Brillouin imaging of the crystalline lens

To test the possibility of measuring the lens elasticity in vivo, we performed Brillouin measurements on laboratory mice (C57BL/6 strain). The probe light from a single-frequency laser (532 nm) was focused with an objective lens into the eye of an anesthetized mouse (Fig. 2 *a*). As we moved the animal on a motorized stage, the optical spectrum of scattered light was recorded. Fig. 2 *b* shows some representative Brillouin spectra obtained along the optical axis of the mouse lens at 3 mW of illumination power and 0.5 s of acquisition time. The signal/noise ratio (SNR) was ~70 at the peak of the spectrum. The SNR allowed the Brillouin frequency shift to be determined from each spectrum by peak localization with an accuracy of ~50 MHz. We confirmed that the SNR increased proportionally to the square root of the input optical energy (optical power times the integration time). We found a frequency sensitivity of ~60 MHz/$\sqrt{\text{Hz}}$/$\sqrt{\text{mW}}$ for the characterization of mouse lenses.

For rapid data acquisition in vivo, we operated the system with a reduced integration time of 100 ms and an optical power of 6 mW. The spectral acquisition speed was 0.1 s, compared with 10 s for our earlier prototype (23) and 10 min for typical FP interferometers (24) used for similar samples ex vivo. The improved data acquisition speed enabled us to obtain a volumetric Brillouin map of the lens in an anesthetized mouse. The cross-sectional images in Fig. 2 *c* span areas of 1.7 × 2 mm^2 (*XY*), 1.8 × 3.1 mm^2 (*YZ*), and 2 × 3.5 mm^2 (*XZ*). With a sampling interval of 100 μm, it took ~2 s to scan each axial line (20 pixels), ~50 s for a cross-sectional area (20 × 25 pixels), and ~20 min over an entire 3D volume. These images visualize, for the first time in vivo (to our knowledge), the gradient of modulus increasing from the outer cortex to inner nucleus, consistent with previous mechanical and ultrasound measurements of excised lens tissues (22).

Age-related stiffening of murine lens in vivo

Using in vivo Brillouin microscopy, we investigated the natural age dependence of the lens modulus. Our examination of two mice (1 and 18 months old, respectively) showed a noticeable difference in their Brillouin axial profiles (Fig. 3 *a*). Besides the expected size difference, the peak Brillouin shift observed at the center of the lens nucleus in

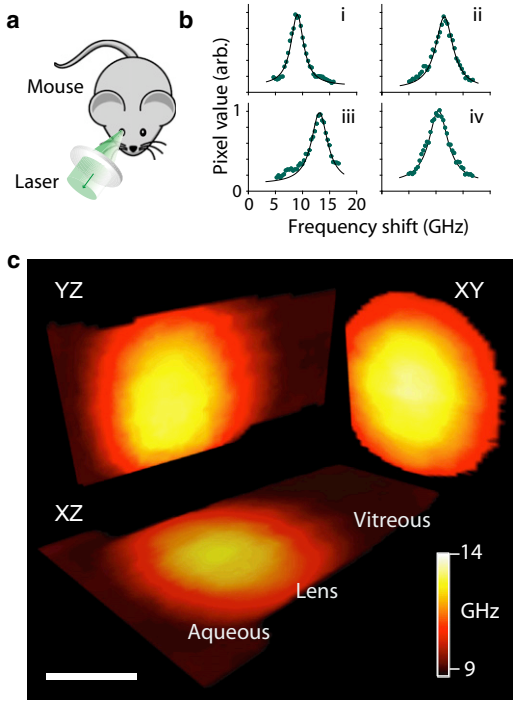

FIGURE 2 In vivo Brillouin imaging of the mouse eye. (*a*) Setup. (*b*) Representative Brillouin spectra taken along the optics axis of the eyeball at depths of 1550 μm (i), 1200 μm (ii), 950 μm (iii), and 550 μm (iv). (*c*) Brillouin elasticity map of a murine eye in vivo. Scale bar: 1 mm.

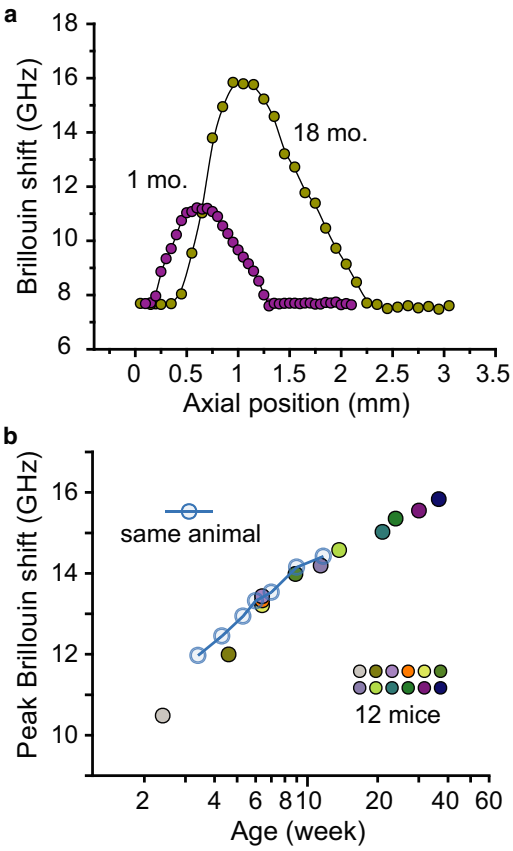

FIGURE 3 Age-related stiffening of the crystalline lens. (*a*) Axial Brillouin profile of the eye in 1-month-old and 18-month-old mice. (*b*) Peak frequency shifts of the lens nucleus in vivo measured from individual mice at various ages (*solid circles*) and one mouse over time (*open circles*).

the old mouse was 16 GHz, whereas the shift in the younger mouse was 11.5 GHz. We extended the study to 12 mice of different ages to find an evident trend of age-related stiffening (Fig. 3 *b*). Next, we imaged one mouse every week for 2 months and obtained consistent age-related data (Fig. 3 *b*). Our results indicate a quantitative (linear-log) relationship between the hypersonic elastic modulus and the animal age. Also, the consistent age-related trend provides evidence for the safety and repeatability of the measurement method.

Age-related stiffening of porcine lens ex vivo

Porcine lenses are known to be a reasonably good model for human lenses in terms of mechanical properties (31). To investigate age-related stiffening of the porcine lens, we measured the Brillouin axial profile of lenses freshly harvested from pigs of different ages (young: <1 month; old: 6 months). The results are shown in Fig. 4. As in the murine lenses, we observed the expected size difference between the lenses and an increase in peak Brillouin shift at the center of the lens nucleus from 9.86 GHz in the young pig to 10.34 GHz in the old pig. The age-related change of Brillouin shift in the pig is apparent but less pronounced than that in the mice. Another interesting observation is related to the shape of the Brillouin depth profile. In the young lens the axial profile follows an almost perfect parabolic curve, but in the older sample the profile seems to reach a plateau in the lens nucleus.

Age-related stiffening of bovine lens ex vivo

We also investigated the age-related stiffening of bovine lenses ex vivo. We measured the Brillouin moduli of bovine lenses freshly harvested from animals in two age groups (young: <1 month; old: 1–2 years, $N = 40$). For direct comparison, we also performed on the same specimens two standard mechanical techniques: a quasi-static stress-strain test to measure the Young's moduli, and dynamic shear rheometry for shear moduli in the frequency range of 0.01–100 Hz (see Supporting Material). We observed statistically significant age-related increases of the modulus with all three methods (Fig. 5). The measured Young's and shear mechanical moduli of the whole bovine lenses ranged between 1 and 100 kPa, whereas the Brillouin moduli were on the order of GPa. Given the physical nature of the Brillouin modulus, which is distinct from conventional low-frequency mechanical moduli, the large difference in their absolute values is not surprising. However, is not obvious whether there should be a quantitative relationship between these parameters, which differ from each other by several orders of magnitude. We therefore sought to investigate this issue, as described below.

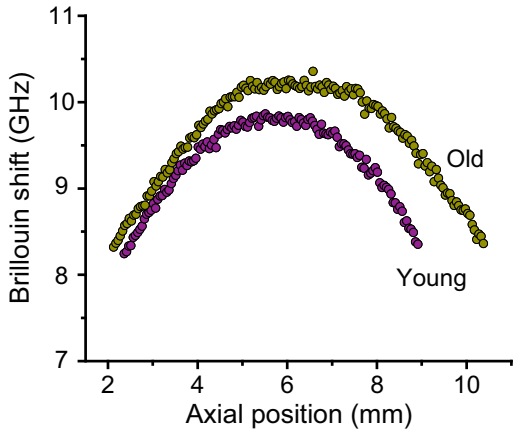

FIGURE 4 Brillouin depth profiles along the optic axis of the porcine lens harvested from young (<1 month) and old (>6 months) animals.

Correlation between Brillouin and low-frequency moduli

Most biological and polymeric materials exhibit viscoelastic properties characterized by frequency-dependent moduli (32). Slower relaxation processes have little time to respond to fast mechanical or acoustic modulation, such as GHz acoustic phonons, and thus hardly contribute to the softness of the material. As a consequence, the modulus tends to increase with the frequency. In addition, the propagation of acoustic phonons is governed by the longitudinal modulus, which is typically much higher than the Young's or shear modulus owing to the incompressibility (i.e., Poisson's ratio ~0.5) of water. The two effects—finite relaxation time and low compressibility—provide a qualitative explanation for the observed large difference in modulus between the Brillouin and standard mechanical tests (Fig. 5). We set out to explore the possible quantitative relationship between the Brillouin longitudinal moduli and Young's/shear moduli for the lens tissue.

For this study, we cut fresh porcine and bovine lenses at various ages (from 1 to 18 months) into small pieces of sizes our mechanical equipment could handle. We calculated the

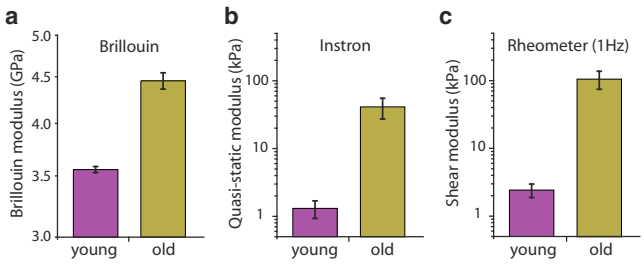

FIGURE 5 Elastic moduli of young and old bovine lenses (*central column*) measured by Brillouin (*a*), longitudinal stress-strain (*b*), and dynamic shear (1 Hz) rheological instruments (*c*); *p*-value = <0.0001, 0.0012, and 0.0016, respectively.

mean Brillouin modulus from the 3D measurement of the Brillouin spectrum and the estimated density and refractive index. A comparison with the Young's modulus measured by a conventional stress-strain test revealed a remarkable correlation between the Brillouin (M') and quasi-static (G') moduli for both porcine and bovine tissues (Fig. 6). A high correlation ($R > 0.9$) was obtained in the curve fit to a log-log linear relationship: $\log(M') = a\ \log(G') + b$, where the fitting parameters were $a = 0.093$ and $b = 9.29$ for porcine tissues and $a = 0.034$ and $b = 9.50$ for bovine tissues.

Recent rheological studies have shown that the mechanical modulus of many soft materials follows a power-law dependence on frequency (ω): $G' \approx G_0\ (\omega/\phi_0)^{\alpha}$, in agreement with the structural damping and soft glassy rheology models. Here, G_0 and Φ_0 are scale factors for stiffness and frequency with magnitudes in the order of 100 kPa and 100 MHz, respectively, and α is the scaling exponent or a trapping factor ($\alpha = 0$ for purely elastic and $0 < \alpha < 1$ for viscoelastic materials) (33,34). Investigators have measured $\alpha = 0.75$ in shear moduli of F-actin semiflexible polymers (35) from 0.1 Hz to 10 kHz, and $\alpha = 0.05$–0.75 in cytoskeletons (36) from 0.01 Hz to 1 kHz. Our finding of a log-log correlation suggests that a similar power law may hold for the Brillouin modulus: $M' \approx M_0\ (\omega/\Phi_0)^{\beta}$, where M_0, Φ_0, and β are constant for a specific sample. Treating α and β as sample-dependent parameters (34), we get $M_0 = 10^b\ {G_0}^a$ and $\beta/\alpha = a\ \log(\omega_L/\phi_0)/\log(\omega_H/\Phi_0)$, where ω_L (~1 Hz) and ω_H (~10^{10} Hz) represent the frequencies of mechanical modulation and acoustic phonons, respectively. From the empirical values, M_0 is found to ~50 GPa, and with Φ_0 = ~50–100 GHz, β/α is 0.6 and 0.2 for porcine and bovine specimens, respectively.

From the above log-log linear relationship, we get $\Delta M'/M' = a\Delta G'/G'$, where $\Delta M'$ and $\Delta G'$ are respective derivatives or variations. For porcine and bovine lenses, we estimated the frequency sensitivity of the Brillouin microscope to be ± 10 MHz/$\sqrt{\text{Hz}}$ at the incident power of 13 mW, which translates into a relative error of $\Delta M'/M' \approx \pm 0.3\%$ at an integration time of 1 s. This indicates that our instrument should be capable of detecting changes in $\Delta G'/G'$ as small as 9% (for $a = 0.032$).

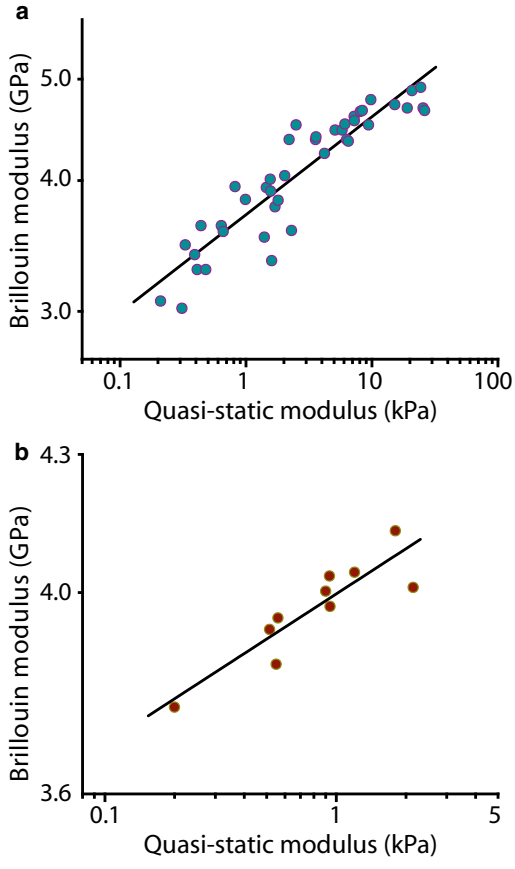

FIGURE 6 Comparison of Brillouin longitudinal and quasi-static Young's moduli of tissue specimens cut from porcine lenses (*a*) and bovine lenses (*b*). Circles, experimental data; solid line, log-log linear fit.

DISCUSSION

The biomechanical and biophysical characteristics of the crystalline lens have long been implicated in the genesis of presbyopia and cataract. The ability to measure these properties in vivo beyond morphology may be useful for prognosis and diagnosis of these disorders, as well as screening for patients at potential risk in refractive surgery and laser vision correction. Traditionally, clinical analysis of the lens has been limited to direct conventional slit lamp microscopy. More recently, newer imaging technologies, such as computer videokeratography, optical coherence tomography, confocal microscopy, ultrasound, and rotating Scheimflug photography, have been employed in the clinical setting. Although these new modalities enhance our understanding of the overall structure of the lens, they do not provide information about the biomechanical and biophysical properties of the lens. Conventional mechanical tests, such as rheology, stress-strain tests, and dynamic mechanical analysis, are destructive. Elastography and ultrasound can interrogate samples nondestructively but generally suffer from limited spatial resolution (millimeter) and mechanical sensitivity (37).

Here, we have demonstrated that Brillouin optical microscopy offers a new way to measure and image the biomechanical and biophysical properties of the eye lens, because it allows one to obtain the local longitudinal modulus of elasticity. In mice, the longitudinal modulus of the crystalline lens varies substantially and gradually from the outer cortex to the nucleus, which is made up of tightly packed fiber layers. Brillouin microscopy allowed us to image the elastic properties of the lens and their changes with age progression in a nondestructive manner.

Our measurements revealed a strong empirical correlation between hypersonic (gigahertz) and low-frequency

moduli within a defined sample group of similar nature (e.g., lens tissues at various locations and/or ages), although the specific relationship differs among different sample types. Remarkably, this correlation was measured to be linear in the log-log scale, which we attributed to the power-law scaling of modulus in frequency. The power-law dependence in shear moduli has been measured in tissues, F-actin polymers, and cellular cytoskeletons at frequencies up to 1 kHz (33,35,38). In the megahertz–subgigahertz regime, the attenuation (i.e., the imaginary part of the complex modulus) of acoustic waves in tissues typically follows a power-law frequency scaling (39), which through the Kramers-Kronig relationship translates into a similar dependence in the elastic modulus (the real part) (40). Taken together, these results indicate that for a given sample type, a log-log linear correlation can be established between the Brillouin and conventional mechanical measurements. Of importance, this suggests that Brillouin microscopy can be used for both comparative and quantitative biomechanical characterizations with judicious interpretation of the data.

In comparison with human lenses, mouse lenses are known to be harder, more spherical, and lacking in accommodation ability. Despite these differences, however, mice and other small animals are useful experimental models to study the genesis of cataract formation (41), evaluate new drugs to slow or ultimately prevent the progression of presbyopia and cataract, and develop treatment procedures to restore some accommodative power (42). Our Brillouin and mechanical measurements on porcine, bovine, and murine lenses showed statistically significant age-related variations in the lens modulus (17–21). The topic of age-related stiffening of the lens and its relation to the etiology of presbyopia has attracted much attention. Recent measurements obtained by Brillouin spectroscopy on human lenses ex vivo showed no measurable dependence of longitudinal nuclear modulus on age progression between 30 and 70 years of age (25). Nevertheless, it will be interesting to see whether the superior data acquisition speed and the imaging capability of the Brillouin system we have demonstrated here will enable us to detect any consistent age-related difference in vivo. On the other hand, in a recent study using rheometry, Schachar et al. (12) questioned the validity of previous mechanical measurements of age-related nuclear sclerosis or an increase in modulus, and proposed that equatorial growth of the lens may be a more significant factor causing presbyopia. Stiffness is an extrinsic mechanical property governed by the spatial distribution of the elastic modulus; therefore, even with no change in the peak elastic modulus in the nucleus, the increasing size of the lens with age alone can result in a substantial increase of the overall stiffness of the lens. In this respect, the ability of Brillouin microscopy to map the elastic modulus with high spatial resolution could help resolve the controversies regarding the biomechanical causes of presbyopia. For example, the Brillouin profile of the porcine lens reveals the flattening of the elastic modulus distribution in the nucleus (Fig. 4). Integrating Brillouin moduli over the lens volume in an appropriate way may provide quantitative information on the stiffness of the lens.

An interesting next step would be to build a clinically viable Brillouin microscope. Infrared light (e.g., at 800 nm) at an illumination power of a few milliwatts or less would be adequate and safe. In vivo Brillouin microscopy may prove useful for clinical diagnosis as well as in basic and preclinical studies.

CONCLUSIONS

In conclusion, we have demonstrated high-resolution measurement of the elastic modulus of the eye lens in live mice. We identified the gradient of elastic modulus in the crystalline lens and observed its age-related increase in vivo. Brillouin microscopy may be used for comparative and quantitative evaluations of biomechanical changes in basic biological research and clinical settings.

SUPPORTING MATERIAL

Additional text, references, and four figures are available at http://www.biophysj.org/biophysj/supplemental/S0006-3495(11)00950-7.

We thank R. Langer, J. Nichol, G. Mckinley, and J. Soulages of the Massachusetts Institute of Technology for providing access to the mechanical test equipment.

This work was supported by grants from the National Institutes of Health (R21EB008472), National Science of Foundation (CBET-0853773), Department of Defense (FA9550-04-1-0079), Center for Integration of Medical Innovation and Technology, and Milton Foundation. G.S received financial support from the Tosteson Fellowship.

REFERENCES

1. Artal, P., and J. Tabernero. 2008. The eye's aplanatic answer. *Nat. Photonics.* 2:586–589.
2. Bloemendal, H. 1977. The vertebrate eye lens. *Science.* 197:127–138.
3. Augusteyn, R. C. 2010. On the growth and internal structure of the human lens. *Exp. Eye Res.* 90:643–654.
4. Benedek, G. B. 1971. Theory of transparency of the eye. *Appl. Opt.* 10:459–473.
5. Delaye, M., and A. Tardieu. 1983. Short-range order of crystallin proteins accounts for eye lens transparency. *Nature.* 302:415–417.
6. Xia, J. Z., Q. H. Wang, …, J. Clauwaert. 1996. Structural basis of eye lens transparency: light scattering by concentrated solutions of bovine α-crystallin proteins. *Biophys. J.* 71:2815–2822.
7. Ethier, C. R., M. Johnson, and J. Ruberti. 2004. Ocular biomechanics and biotransport. *Annu. Rev. Biomed. Eng.* 6:249–273.
8. Heys, K. R., S. L. Cram, and R. J. W. Truscott. 2004. Massive increase in the stiffness of the human lens nucleus with age: the basis for presbyopia? *Mol. Vis.* 10:956–963.
9. McGinty, S. J., and R. J. W. Truscott. 2006. Presbyopia: the first stage of nuclear cataract? *Ophthalmic Res.* 38:137–148.

10. Glasser, A., and M. C. W. Campbell. 1999. Biometric, optical and physical changes in the isolated human crystalline lens with age in relation to presbyopia. *Vision Res.* 39:1991–2015.

11. Weeber, H. A., G. Eckert, …, R. G. van der Heijde. 2005. Dynamic mechanical properties of human lenses. *Exp. Eye Res.* 80:425–434.

12. Schachar, R. A., R. W. Chan, and M. Fu. 2011. Viscoelastic properties of fresh human lenses under 40 years of age: implications for the aetiology of presbyopia. *Br. J. Ophthalmol.* 95:1010–1013.

13. Weeber, H. A., and R. G. L. van der Heijde. 2007. On the relationship between lens stiffness and accommodative amplitude. *Exp. Eye Res.* 85:602–607.

14. Heys, K. R., and R. J. W. Truscott. 2008. The stiffness of human cataract lenses is a function of both age and the type of cataract. *Exp. Eye Res.* 86:701–703.

15. Glasser, A. 2008. Restoration of accommodation: surgical options for correction of presbyopia. *Clin. Exp. Optom.* 91:279–295.

16. Burd, H. J., G. S. Wilde, and S. J. Judge. 2011. An improved spinning lens test to determine the stiffness of the human lens. *Exp. Eye Res.* 92:28–39.

17. Fisher, R. F. 1971. The elastic constants of the human lens. *J. Physiol.* 212:147–180.

18. Glasser, A., and M. C. W. Campbell. 1998. Presbyopia and the optical changes in the human crystalline lens with age. *Vision Res.* 38: 209–229.

19. Weeber, H. A., G. Eckert, …, R. G. van der Heijde. 2007. Stiffness gradient in the crystalline lens. *Graefes Arch. Clin. Exp. Ophthalmol.* 245:1357–1366.

20. Baradia, H., N. Nikahd, and A. Glasser. 2010. Mouse lens stiffness measurements. *Exp. Eye Res.* 91:300–307.

21. Erpelding, T. N., K. W. Hollman, and M. O'Donnell. 2007. Mapping age-related elasticity changes in porcine lenses using bubble-based acoustic radiation force. *Exp. Eye Res.* 84:332–341.

22. De Korte, C. L., A. F. W. Van Der Steen, …, G. J. Puppels. 1994. Relation between local acoustic parameters and protein distribution in human and porcine eye lenses. *Exp. Eye Res.* 59:617–627.

23. Scarcelli, G., and S. H. Yun. 2008. Confocal Brillouin microscopy for three-dimensional mechanical imaging. *Nat. Photonics.* 2:39–43.

24. Vaughan, J. M., and J. T. Randall. 1980. Brillouin scattering, density and elastic properties of the lens and cornea of the eye. *Nature.* 284:489–491.

25. Bailey, S. T., M. D. Twa, …, R. Sooryakumar. 2010. Light-scattering study of the normal human eye lens: elastic properties and age dependence. *IEEE Trans. Biomed. Eng.* 57:2910–2917.

26. Scarcelli, G., P. Kim, and S. H. Yun. 2008. Cross-axis cascading of spectral dispersion. *Opt. Lett.* 33:2979–2981.

27. Scarcelli, G., and S. H. Yun. 2011. Multistage VIPA etalons for high-extinction parallel Brillouin spectroscopy. *Opt. Express.* 19:10913–10922.

28. Pierscionek, B. K., A. Belaidi, and H. H. Bruun. 2005. Refractive index distribution in the porcine eye lens for 532 nm and 633 nm light. *Eye (Lond.).* 19:375–381.

29. Pierscionek, B. K. 1994. Refractive index of decapsulated bovine lens surfaces measured with a reflectometric sensor. *Vision Res.* 34:1927–1933.

30. Pierscionek, B. K. 1995. The refractive index along the optic axis of the bovine lens. *Eye (Lond.).* 9:776–782.

31. Schachar, R. A., R. W. Chan, and M. Fu. 2007. Viscoelastic shear properties of the fresh porcine lens. *Br. J. Ophthalmol.* 91:366–368.

32. Mofrad, M. R. K., and R. D. Kamm, editors. 2006. Cytoskeletal Mechanics. Cambridge University Press, New York.

33. Fabry, B., G. N. Maksym, …, J. J. Fredberg. 2001. Scaling the microrheology of living cells. *Phys. Rev. Lett.* 87:148102.

34. Sollich, P., F. Lequeux, …, M. E. Cates. 1997. Rheology of soft glassy materials. *Phys. Rev. Lett.* 78:2020–2023.

35. Gittes, F., and F. C. MacKintosh. 1998. Dynamic shear modulus of a semiflexible polymer network. *Phys. Rev. E Stat. Phys. Plasmas Fluids Relat. Interdiscip. Topics.* 58:R1241–R1244.

36. Discher, D., C. Dong, …, S. Weinbaum. 2009. Biomechanics: cell research and applications for the next decade. *Ann. Biomed. Eng.* 37:847–859.

37. Greenleaf, J. F., M. Fatemi, and M. Insana. 2003. Selected methods for imaging elastic properties of biological tissues. *Annu. Rev. Biomed. Eng.* 5:57–78.

38. Deng, L. H., X. Trepat, …, J. J. Fredberg. 2006. Fast and slow dynamics of the cytoskeleton. *Nat. Mater.* 5:636–640.

39. Duck, F. A. 1990. Physical Properties of Tissue. Academic Press, London.

40. Holm, S., and R. Sinkus. 2010. A unifying fractional wave equation for compressional and shear waves. *J. Acoust. Soc. Am.* 127:542–559.

41. Nishimoto, S., K. Kawane, …, S. Nagata. 2003. Nuclear cataract caused by a lack of DNA degradation in the mouse eye lens. *Nature.* 424:1071–1074.

42. Sistla, P. A., M. A. Reilly, …, N. Ravi. 2009. The effect of R120G mutation in αB-Crystallin on the mechanical properties of mouse lenses. *Proc. ARVO Reducing Disparit. Eye Dis. Treat.*, Ft. Lauderdale, FL. Abstract 2107.

Supporting Materials for

In vivo measurement of age-related stiffening in the crystalline lens by Brillouin optical microscopy

Giuliano Scarcelli, Pilhan Kim, Seok Hyun Yun*

*E-mail: syun@hms.harvard.edu

1. Double VIPA spectrometer.

A VIPA etalon disperses the spectrum of light along a linear axis. Two or more VIPA etalons can be cascaded with the cross-axis configuration to improve the extinction. It can be shown that the extinction or contrast C_N of a cross-axis cascade of N identical etalons is given by: $\log(C_N) \approx N*\log(4F^2/\pi^2)$, where F denotes the finesse of each etalon.

We built a two stage VIPA spectrometer with two VIPA etalons where the grating axes of the etalons are crossed at 0 (vertical to the optical table), 90 (horizontal) degrees, respectively. Due to the combined dispersion along the horizontal and vertical direction, the Brillouin spectrum appears tilted on the diagonal direction at about 45 degrees (Fig. S1). Between the two etalons, we employed a relay telescope and a square-hole spatial mask that transmitted only the Brillouin-shifted frequencies within the spectral transfer function, thereby suppressing Fresnel reflection and elastic scattering at each stage. The extinction of the 2-stage setup was 58 dB with FWHM spectral resolution of 0.8 GHz and the total insertion loss of a Brillouin signal was ~4 dB. The high extinction ratio allowed us to move from the previous low-NA dual-axis configuration to a high-NA *epi* configuration in the Brillouin microscope, thereby improving the signal collection efficiency. Furthermore, the contrast improvement enabled us to detect a small number of Brillouin photons coming from the tissue using a state-of-the-art electron-multiplying (EM) CCD.

Figure S1 shows unprocessed data recorded *in vivo* by the camera in the spectrometer at different depths along the ocular optic axis of the mouse lens, featuring the spectral signatures of anterior cortex, lens nucleus, posterior cortex and vitreous humor, respectively.

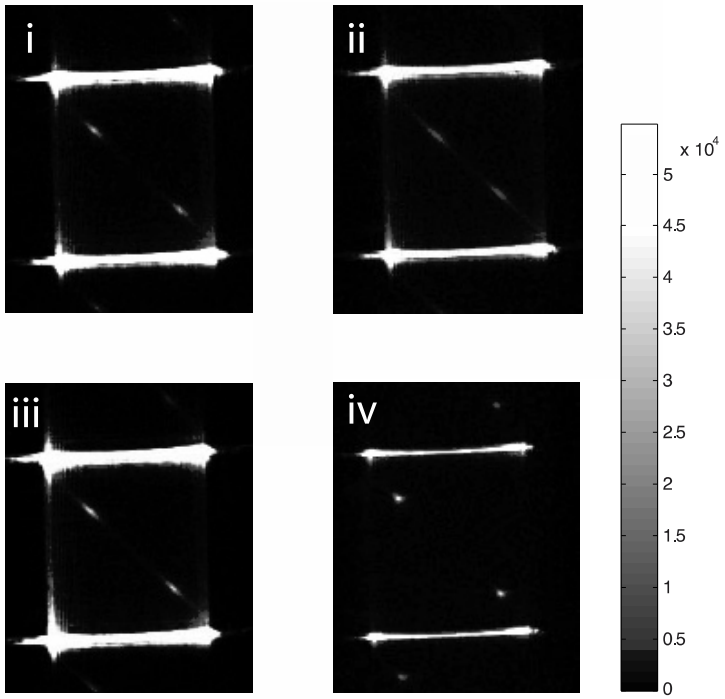

Fig. S1. Raw spectrometer data showing the Stokes and anti-Stokes peaks taken along the optics axis of the eyeball at different depths of 250 μm (i), 550 μm (ii), 1050 μm (iii), and 1450 μm (iv).

2. Various types of modulus of elasticity.

In an isotropic material, Young's modulus, E, is defined as the ratio between an applied axial or longitudinal stress and resulting axial strain. To a good approximation, this quantity can be measured by compressive or tensile stress-strain tests.

The bulk modulus, K, is a useful parameter to describe liquids as it refers to the situation where the material is uniformly loaded and all the strains normal to the stress direction are equal. It is defined as the ratio of applied stress, or pressure, to volume change and can be expressed in terms of Young's modulus and Poisson's ratio as $K=E/3(1-2\sigma)$.

Shear modulus describes a situation where all the strains perpendicular to the stress direction are zero, i.e. alterations in material shape are induced without involving a volume change. To a good approximation, this situation is created in commercial rheometers (e.g. the one used in our work), or alternatively in ultrasound measurements using shear acoustic waves. The shear modulus, G, is defined as the ratio between shear stress and shear strain.

The longitudinal modulus M is defined as the ratio of axial stress to axial strain. It is different from Young's modulus in that the material perturbation occurs in a strictly uniaxial strain state so that no shear strain is produced. This happens in response to longitudinal acoustic waves, as in the case Brillouin microscopy, where rapidly oscillating and purely longitudinal stresses are induced. The longitudinal modulus is related to the bulk and shear moduli as follows: $M=K+4/3G$. The Brillouin frequency shift is proportional to the velocity of propagation of hypersonic (GHz) acoustic waves inside the material. In principle, both longitudinal and shear waves can be probed by Brillouin spectroscopy. However, for an isotropic material Brillouin scattering due to shear waves is forbidden by phase matching in the backward *epi* detection geometry. Therefore, in our experiments we could measure only the longitudinal moduli, which we refer to as Brillouin moduli.

In contrast to the various types of modulus of elasticity, the stiffness of a sample is an extrinsic mechanical property that not only depends on the elastic moduli of its constituent materials but also on the shape and size of the sample. For example, a thick piece of plastic is likely to have a higher stiffness than a thin piece of plastic of the same elastic modulus. In principle, the stiffness of crystalline lens can be calculated from the spatial map of the elastic modulus.

3. Measurements on animal eye lenses *ex vivo*

Compression stress-strain test

We placed the samples between the two plates of the Instron instrument. We collected raw data controlling the relative compression and measuring the corresponding load, while varying the strain at a constant speed (1% to 5% strain per minute). The thickness and cross-sectional area of each sample was recorded prior to the measurement. We always observed an excellent linear relationship even beyond 10% strain (Fig. S2). We calculated Young's modulus by a linear fit to the stress-strain curve in the first 5% strain.

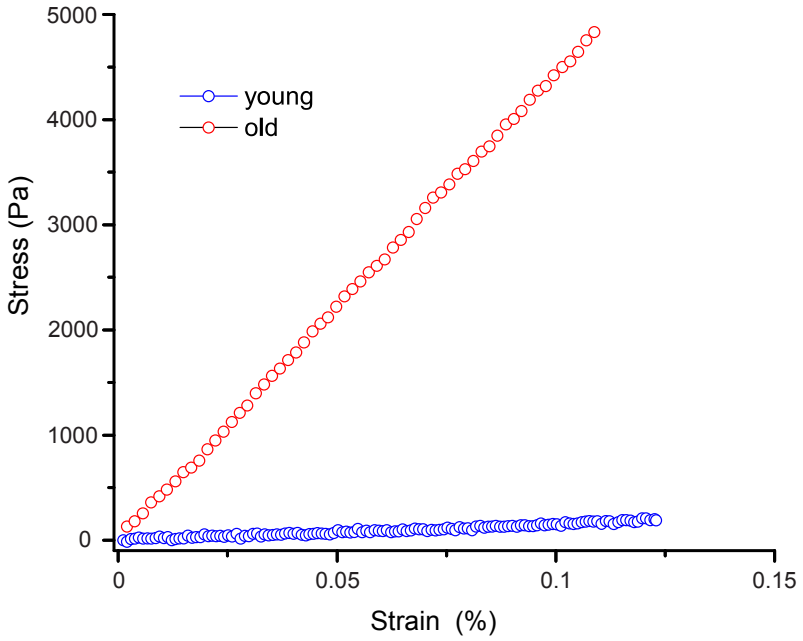

Fig. S2. Representative stress-strain curves for young (blue) vs. old (red) bovine lenses. From the slopes, we found Young's moduli of 1.5 kPa for the young lens and 44 kPa for the old lens.

Shear Rheometry

We used an AR-G2 shear rheometer with 20-mm parallel plate geometry. The sample was placed on the bottom plate at a controlled temperature (23°C). We positioned the upper plate to touch the sample and then further lowered the plate by 200 μm to preload the sample for reliable shear measurement. We waited until the sample relaxed and the monitored normal pressure vanished. First, we ran a sweep of the shear strain between 0.05% and 5% in amplitude to determine the region of strain amplitude with constant behavior. Then, we ran a frequency sweep from 0.1 Hz to 50 Hz at fixed strain amplitude (typically 0.1%). The instrument provided the shear modulus value at each frequency based on the shear stress, strain, and sample size. Figure 5c in the paper depicts the shear moduli at 1 Hz frequency, obtained with the nuclear parts of bovine lenses (6 mm diameter, 3 mm thickness). Representative full sweep data is shown in Fig. S3.

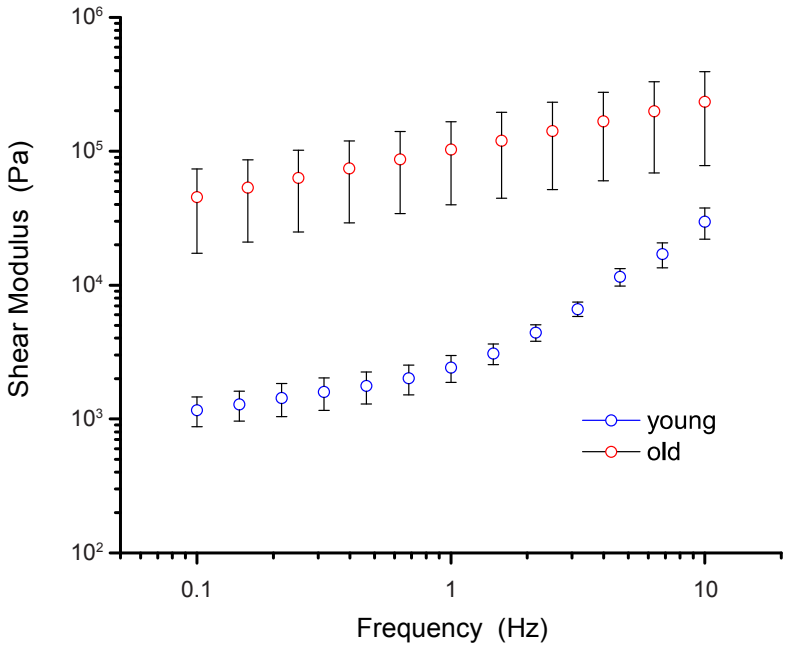

Fig. S3. Typical Shear moduli of the nucleus of a young (blue) and old (red) bovine lens in the mechanical frequency range of 0.1 to 10 Hz.

In our experiments, the shear modulus measured by rheometry (at 1 Hz) was found to be generally higher than the Young's modulus measured by the quasi-static strain-stress test. We believe this observation was primarily due to our specific experimental conditions. For example, the samples were preloaded with 5-10% longitudinal strain prior to the shear measurement, whereas the Young's modulus was calculated in the longitudinal strain of 0 to 5%.

4. Effect of refractive index and density variation on Brillouin modulus estimation

In our analysis of Brillouin modulus, for example in Fig. 6a, we assumed a constant value for ρ/n^2 for all lens samples. In fact, those small pieces of tissue have slightly different refractive indices and density values. In order to estimate the error due to our assumption in the analysis, we performed the following analysis.

For porcine crystalline lenses, the profile of the refractive index has been previously measured and available in the literature, and the local value of the mass density can be estimated accurately by modeling the lens as a mixture of water and crystalline proteins and using Gladstone-Dale formula (1, 2). First, we calculated the Brillouin modulus accounting for the spatial variation of the density and index of refraction. Second, we used ρ=1.13 g/cm^3 and n=1.4, which were calculated from the spatial averages over the whole lens. We found that the difference between these two calculations was less than +/- 2%. Therefore, we conclude that the error due to the assumption of constant ρ/n^2 should be negligible in most cases.

Figure S4 depicts both datasets obtained with the spatial resolved (diamond) and constant (square) values for ρ/n^2 in comparison to the Instron moduli.

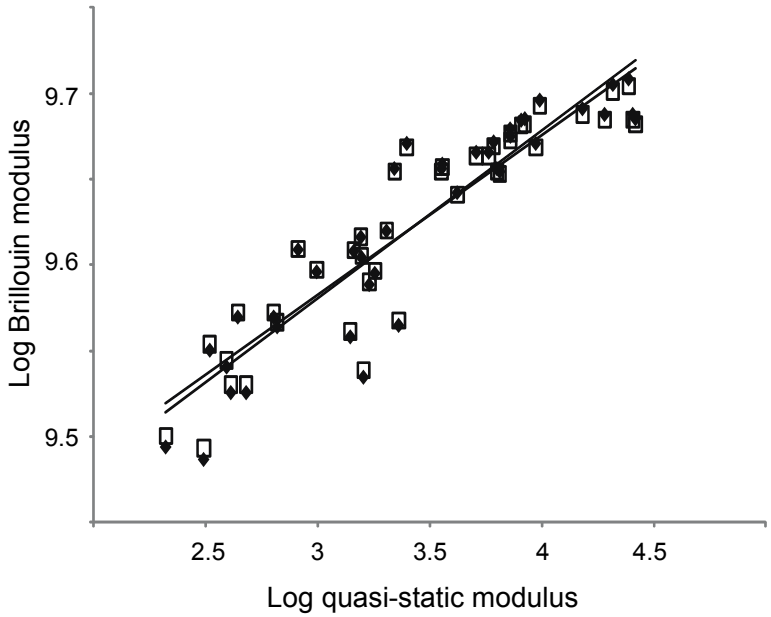

Fig. S4. Index/density correction. Brillouin vs. Instron Young's moduli, when the variation of ρ/n^2 between the samples was considered (solid diamonds) or neglected (hollow squares). Lines are linear fits.

References

1. Pierscionek, B. K., A. Belaidi, and H. H. Bruun. 2005. Refractive index distribution in the porcine eye lens for 532 nm and 633 nm light. Eye 19:375-381.
2. Dekorte, C. L., A. F. W. Vandersteen, J. M. Thijssen, J. J. Duindam, C. Otto, and G. J. Puppels. 1994. Relation between local acoustic parameters and protein distribution in human and procine eye lenses. Experimental Eye Research 59:617-627.